Article:
Shepherd, JS, Fairweather, M, Heggs, PJ et al. (1 more author) (2015) Mathematical modelling of the pre-oxidation of a uranium carbide fuel pellet. Computers and Chemical Engineering, 83. 203 - 213. ISSN 0098-1354

https://doi.org/10.1016/j.compchemeng.2015.05.001

Mathematical Modelling of the Pre-Oxidation of a Uranium Carbide Fuel Pellet

James Shepherd*, Michael Fairweather, Peter Heggs, Bruce Hanson

School of Chemical and Process Engineering

University of Leeds, Leeds, LS2 9JT, UK

js08js@leeds.ac.uk

+44113 343 2543

Abstract

Uranium carbide is a candidate fuel for future nuclear reactors. However, for it to be implemented in a closed fuel cycle, an outline for its reprocessing is necessary. One proposed method is to oxidise the uranium carbide into uranium oxide which can then be reprocessed using current infrastructure. A mathematical model describing the heat and mass transfer processes involved in such an oxidation has been constructed. The available literature was consulted for reaction coefficients and information on reaction products. A stable and convergent numerical solution has been developed using a combination of finite-difference approximations of the differential equations. Completion times of approximately 3-30 hours are predicted given a spherical pellet with a radius of 9.35 mm under varying initial conditions. The transient temperature distribution throughout the system is predicted, with a maximum temperature of 1458°C observed from an initial temperature of 500°C at an oxygen concentration of 3.15 $mol\ m^{-3}$.

Keywords: Uranium Carbide; Oxidation; Finite-difference techniques; Heat and mass transfer

Nomenclature

Symbol	Description	Units
A	Surface area of the uranium carbide pellet	m^2
C_{CO}	Carbon monoxide concentration	$mol\ m^{-3}$
C_{O_2}	Oxygen concentration	$mol\ m^{-3}$
$C_{O_2}^B$	Bulk gas oxygen concentration	$mol\ m^{-3}$
D	Cylindrical pellet diameter	m
d_e	Spherical pellet diameter	m
E_A	Activation energy of the reaction at the carbide surface	$J\ mol^{-1}$
h	Heat transfer coefficient	$W\ m^{-2}\ K^{-1}$
i	An integer representing the radial increment, $1 \leq i \leq k$	
k	An integer representing the maximum value of i; its value at the solid surface	
k_C	First order reaction coefficient	$m\ s^{-1}$
k_{fluid}	Thermal conductivity of surrounding fluid	$W\ m^{-1}\ K^{-1}$
k_g	Mass transport coefficient	$m\ s^{-1}$
k_{UC}	Thermal conductivity of uranium carbide	$W\ m^{-1}\ K^{-1}$
k_1	A constant representing the maximum value of k_C	$m\ s^{-1}$
L	Cylindrical pellet length	m
n	An integer designating the current time step, $n \geq 1$	
Nu	Nusselt number	
n_{UC}	Number of moles of uranium carbide	mol
p	Pressure	atm
Pr	Prandtl number	
r	Radius within solid	m
R_C	Rate of oxygen consumption at the reaction interface	$mol\ s^{-1}$
R_C^*	Rate of oxygen transfer across the external gas film layer	$mol\ s^{-1}$
R	Gas constant	$J\ mol^{-1}\ K^{-1}$
Re	Reynolds number	
r_1	Radius of the carbide pellet	m
Sc	Schmidt number	
Sh	Sherwood number	

t	Time passed since oxidation started	s
T	Solid temperature	K
T^B	Bulk gas temperature	K
u_1, u_2, u_3	Solutions at the increment sizes h_1, h_2 and h_3 respectively	
u	Estimated solution using infinitely small increment sizes	
V	Total volume of the bulk gas surrounding the oxidising pellet	m^3

Greek Symbol

α	Thermal diffusivity	$m^2\ s^{-1}$
ΔH_R	Enthalpy of oxidation at carbide surface	$J\ mol^{-1}$
Ω	Collison integral	
ε	Emissivity of uranium carbide	
μ	Fluid dynamic viscosity	$kg\ m^{-1}\ s^{-1}$
ρ_o	Fluid density	$kg\ m^{-3}$
σ	Stefan-Boltzmann constant	$W\ m^{-2}\ K^{-1}$
σ_{O_2-CO}	Constant in the Lennard-Jones potential formula	Å

1 Introduction

Uranium carbide (UC) is a candidate fuel for use in Generation IV nuclear reactors [1, 2]. Its appeal stems from a high thermal conductivity compared to the oxide form [3, 4] allowing for easier regulation of fuel bed temperatures, and a higher density of heavy metal atoms making it a better plutonium breeder – an invaluable characteristic for fast reactor fuel.

One drawback, however, is that upon dissolution in nitric acid, a step in the PUREX (Plutonium Uranium Redox Extraction) method for oxide fuel reprocessing, organic compounds are formed in solution from the displaced carbon. These organics, in particular carboxylic and mellitic acid [5, 6], can then complex the uranium and plutonium ions in the resulting solution making their extraction significantly less effective and consequently wasting valuable fissile material. Therefore, in order for carbide fuels to be reprocessed in the same manner as oxide fuels, and hence be simpler and less expensive to introduce, the problem of organics in solution must be addressed.

The oxidation of uranium carbide to uranium oxide prior to dissolution in nitric acid is one proposed solution, allowing the fuel to then be reprocessed as normal. However, it is not without its own difficulties. The oxidation in air is known to be highly exothermic [7, 8], especially if the carbide is in powder form [9], resulting in the risk of thermal runaway and the possibility of self-ignition.

The model described in this paper aims to simulate the oxidation of a uranium carbide fuel pellet in air and predict the temperatures reached by the pellet under different initial conditions. Such a model would then be of use in outlining the necessary safety conditions for both general handling of carbides and the oxidation itself.

The oxidation, assumed to be taking place in air, can be written as the following two-step reaction:

$$2UC(s) + 3O_2(g) \rightarrow 2UO_2(s) + 2CO(g) \quad (1)$$

$$2CO(g) + O_2(g) \rightarrow 2CO_2(g) \quad (2)$$

The initial oxidation, Eq. (1), is a heterogeneous reaction taking place at the surface of the carbide pellet and produces carbon monoxide and uranium dioxide. The carbon monoxide is then further oxidised to carbon dioxide by a homogeneous reaction in the bulk gas, Eq. (2).

The oxide product layer is assumed to instantaneously spall off from the carbide pellet surface. It is unclear in the literature whether or not this is the case. Some reports suggest it adheres to the pellet [10], which slows the reaction due to diffusion across the oxide layer, whilst Mazaudier *et al.* [11] observe that no product layer adheres: perhaps due to the marked decrease in density from *UC* (13.6 g/cm^3) to UO_2 (11.0 g/cm^3), which causes a significant volume expansion of approximately 33%.

This assumption, of an instantaneously spalling oxide product layer, allows the oxidation kinetics to be simply represented by Eq. (1) and (2). It is observed by Berthinier *et al.* [12, 13] that further oxidation of the UO_2 occurs under most conditions, producing higher oxides such as U_3O_8 and U_3O_7. However, since the UO_2 produced in the initial surface reaction is assumed to spall off, as suggested by Mazaudier *et al*. [11], and hence not be present in this model, these further oxidations are not considered.

The enthalpy of reaction for the overall reaction given in Eqs. (1) and (2) was calculated theoretically to be -1380 kJ/mol, falling within the reported range of -1260 to -1500 kJ/mol [7]. The initial oxidation reaction, Eq. (1), is taken to be first order, and is assumed to occur only at the surface of the carbide with no penetration of the carbide by the oxidising gas. This reaction has an enthalpy calculated to be -1098 kJ/mol. Part of the heat generated at the reaction interface by Eq. (1) is then conducted into the UC pellet, with the remainder transfers to the bulk gas via both convection and radiation.

The density increase from the carbide fuel to the oxide product, plus the fact that gas is formed at the interface between the two materials, is assumed to prevent an oxide layer adhering. The model is therefore a variation, but of a similar form as, the shrinking core model [14].

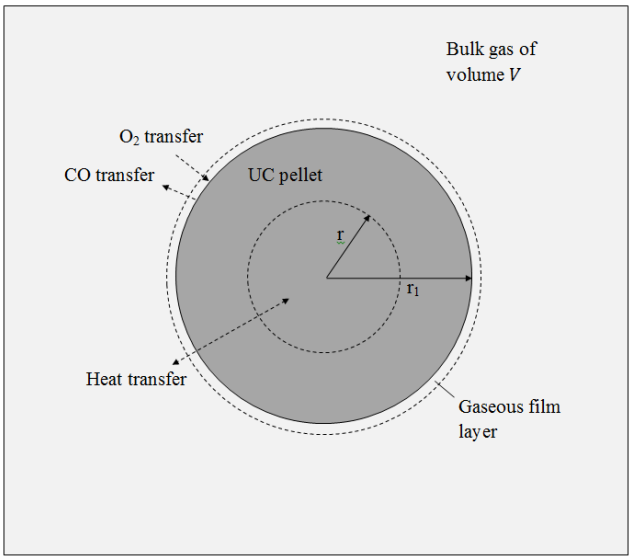

Fig. 1. A one dimensional approximation of a UC pellet as an equivalent volume sphere.

At the surface of the carbide, i.e. where $r = r_1$, heat transfer between the solid and the bulk oxidising gas is included. The bulk gas can be assumed to be either an infinite medium at a constant temperature, or a finite volume with a variable temperature. In either case, however, there is no oxidant depletion during the reaction, the fluid is assumed to be stagnant and atmospheric pressure is assumed. The assumption of an infinite gaseous oxidant is removed at a later point to examine the effects of the secondary oxidation on the bulk gas composition, but should be assumed to be in place unless stated otherwise.

Oxygen transfers from the bulk gas to the reaction interface by diffusing through a gaseous film layer, assumed to comprise produced carbon monoxide, where it is consumed in the reaction given by Eq. (1). For the system shown in Figure 1, Figure 2 is a schematic of the radial oxygen and carbon monoxide profiles through the gaseous film layer depicted in former figure. Additionally, Figure 3 is a schematic of the radial temperature distribution. In both figures, the initial conditions are shown at time $t = 0$. The profiles are then shown at a later time $t = t_1$ and then at a further time $t = t_2$, where $t_2 > t_1$.

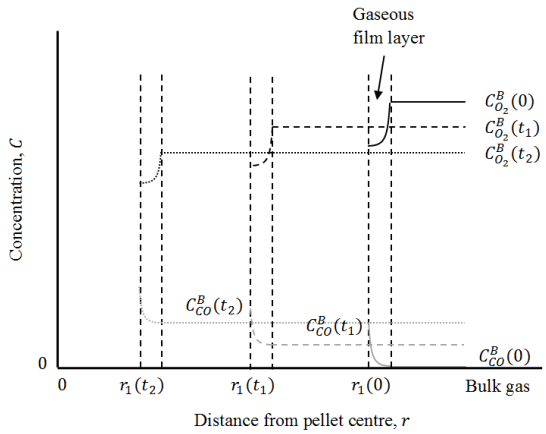

Fig. 2. The radial oxygen and carbon monoxide concentration profiles at three different instances during the reaction.

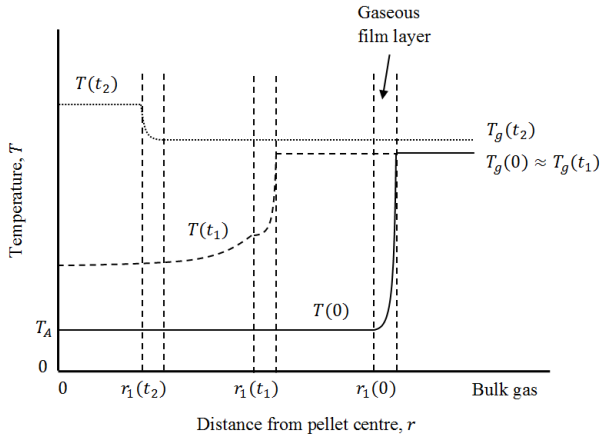

Fig. 3. The radial temperature profiles at three different instances during the reaction.

In Figure 2, neither gas is present at $r < r_1$ due to the carbide being assumed to be non-porous. Oxygen is consumed and carbon monoxide generated at the reaction interface, $r = r_1$. If a finite volume of reactant gas is assumed, the bulk concentration of oxygen will deplete over time as shown. Depending on the temperature, the bulk concentration of carbon monoxide will increase. This change in the composition of the bulk gas is discussed further in section 2.2.

In Figure 3, it can be seen that at time $t = 0$, the pellet is at ambient temperature. A short time later at $t = t_1$, a temperature gradient exists within the pellet due to sudden exposure of the pellet to the hotter bulk gas. After the reaction has been occurring for some time, at $t = t_2$, the pellet has become roughly isothermal due to the high thermal conductivity of uranium carbide and the more incremental nature of the temperature changes at the pellet surface. Due to the heat generated by the reaction, the pellet is now hotter than the bulk gas meaning that, depending on the gas volume, the bulk gas will heat up.

In both Figures 2 and 3, the radial decrease of the carbide pellet over time is illustrated. A thickness for the gaseous film layer is not necessary as the layer is present in the model to simply represent the resistance to the mass and heat transfer between the bulk gas and the pellet and is contained within the heat and mass transfer coefficients.

This summary provides a transient description of the temperature throughout the solid for the course of the reaction. Using this information, the reaction rate at the surface can be calculated as well as how the size of the pellet reduces over time.

Similar models are scarce in the present literature, with only one model found for the oxidation of uranium carbide [15]. Scott [15] modelled the oxidation of spherical graphite fuel pellets in a fixed or moving bed, using a shrinking core method for the individual pellets in one dimension. The limiting process was found to be the diffusion of oxygen through the adherent uranium oxide layer to the carbide surface. Scott [15] calculated the rate of this diffusion by assuming the oxygen concentration at the oxide-carbide interface to be zero, since it is the limiting process, and then calculated the concentration gradient at the interface from the oxygen concentration at the outer surface of the oxide layer. This work therefore assumed that the reaction rate is controlled by a combination of the diffusion of oxygen through this product layer and through an external gas film surrounding the solid.

The present model provides a more detailed numerical method of oxidising uranium carbide, and also removes the assumption that an adherent oxide layer will form on the pellet. Mass transfer is therefore only considered to occur across the gas film layer surrounding the solid.

The non-linear set of coupled heat and mass partial differential equations comprising the model have been solved numerically through finite-difference approximations of the relevant differential equations and boundary conditions. The set of equations produced as a result were then solved using original software written in FORTRAN 95.

The bulk of the mathematical equations used to model the physical processes that occur during the oxidation are detailed in the following section, Section 2. The numerical methods used to solve these equations are covered in Section 3, with the results and conclusions being presented in Sections 4 and 5, respectively.

2 Mathematical Representation

The model can be thought of as a set of distinct, but dependent, sections, each requiring a solution for every time step, n:

1. Heat and mass transfer across an external gas film around the pellet.
2. Heat flow into the solid uranium carbide.
3. The resulting reaction rate at the uranium carbide surface.
4. The resulting decrease in size of the pellet.

Before the mathematical equations describing these processes are outlined, the geometry of the pellet being modelled should first be characterised. The pellet is assumed to be the equivalent volume sphere, as depicted in Fig. 1, of a right circular cylinder with a diameter equal to its length (i.e. an orthocylinder). This assumption was made as the pellets currently in use in fuel pins are roughly right cylinders with their exact dimensions varying depending on the fuel and reactor type used.

The diameter of an equivalent volume sphere is defined as 6 multiplied by the ratio of the volume to the surface area and for a cylindrical pellet is given by the following equation:

$$d_e = 6D/[2D/L + 4] \tag{3}$$

where d_e is the diameter of the equivalent volume sphere, D is the diameter of the cylinder and L is the length of the cylinder.

Hence for an orthocylinder, where $D = L$, Eq. (3) reduces to:

$$d_e = D \tag{4}$$

Importantly, the initial volume to surface area ratios of the right cylinder and the sphere are equivalent in the case of a right cylinder which allows a justification of the equivalent sphere assumption.

The oxidation reaction described in Eq. (1) is then assumed to be occurring at the surface of the spherical pellet. The reaction kinetics for the oxidation can be written as the following first order equation [15]:

$$R_C = k_C A C_{O_2}\big|_{r_1} \tag{5}$$

where R_C is the rate of oxygen consumption at the carbide surface, A is the surface area of the reacting carbide, $C_{O_2}\big|_{r_1}$ is the oxygen concentration at the carbide surface and k_C, the reaction coefficient, is represented as the following Arrhenius function [15]:

$$k_C = k_1 exp\left(-E_A/RT|_{r_1}\right) \tag{6}$$

where k_1 is a constant provided by Scott [15] as $20000\ gmol\ cm^{-2}\ s^{-1}\ atm^{-1}$, E_A is the activation energy reported to be 7000 $J\ mol^{-1}$ [16], R is the ideal gas constant and $T|_{r_1}$ is the absolute temperature at the carbide surface.

2.1 Heat and Mass Transfer

In order to calculate the reaction rate given by Eq. (5), it is necessary to know both the temperature, $T|_{r_1}$, and concentration of oxidant, $C_{O_2}\big|_{r_1}$, at the reaction interface through the use of heat and mass transfer equations.

The conduction of heat through the solid is represented by the Fourier equation in spherical co-ordinates as:

For $t \geq 0$ and $0 < r \leq r_1(t)$:

$$\frac{\partial T}{\partial t} = \alpha\left(\frac{\partial^2 T}{\partial r^2} + \frac{2}{r}\frac{\partial T}{\partial r}\right) \tag{7}$$

where r is the radius, $r_1(t)$ is the radius to the surface of the reacting carbide, T is the temperature of the uranium carbide, t is the time passed since the start of the oxidation and α is the thermal diffusivity of uranium carbide.

The initial conditions for Eq. (7) are:

For $t \leq 0$:

$$r_1(0) > 0 \tag{8}$$

For $t \leq 0$ and $0 \leq r \leq r_1(t)$:

$$T = T_A \tag{9}$$

where T_A is the ambient temperature, assumed to be $25°C$.

Boundary conditions are then applied to Eq. (7) at the centre and the surface of the spherical pellet.

Due to the symmetry of the sphere, the heat transfer boundary condition at the centre of the sphere is adiabatic, and is expressed as:

For $t \geq 0$ and $r = 0$:

$$\frac{\partial T}{\partial r} = 0 \tag{10}$$

The boundary condition at the surface of the pellet, however, is more complex, requiring consideration of the heat and mass transfer between the solid and the bulk gas across a gaseous film layer assumed to comprise carbon monoxide.

The heat flux experienced by the pellet at the surface can be written as the following boundary condition. Note that the effects of convective and radiative heat transfer, as well as heat generated by the reaction, are the terms involved.

For $t \geq 0$ and $r = r_1$:

$$-k_{UC}\left.\frac{\partial T}{\partial r}\right|_{r_1} = h\left(T|_{r_1} - T^B\right) + \varepsilon\sigma\left(\left(T|_{r_1}\right)^4 - (T^B)^4\right) + \Delta H_R k_C C_{O_2}|_{r_1} \tag{11}$$

where k_{UC} is the thermal conductivity of UC, h is the heat transfer coefficient, T^B is the bulk gas temperature, ε the emissivity of uranium carbide, σ the Stefan-Boltzmann constant and ΔH_R is the enthalpy of the surface reaction, Eq. (1).

The emissivity of uranium carbide is given by De Coninck et al [1] as:

$$\varepsilon = 0.55 - 8.5 \times 10^{-5} T|_{r_1} \tag{12}$$

The heat transfer coefficient is calculated from the Nusselt number according to Eq. (13):

$$h = \frac{k_{fluid} Nu}{2r_1} \tag{13}$$

where k_{fluid} is the thermal conductivity of the fluid, assumed to be air of varying oxygen concentrations, surrounding the pellet, and Nu is the Nusselt number.

Given the assumption that the surrounding fluid is stagnant, i.e. $Re = 0$, the Nusselt number can be expressed as shown in Eq. (14) according to Rowe *et al.* [17]:

$$Nu = 2.0 \tag{14}$$

The thermal conductivity of the fluid, k_{fluid}, for temperatures up to 900°C is provided by Vines [18] as:

$$k_{fluid} \times 10^5 = \frac{0.604\sqrt{T^B}}{1 + \frac{245}{T^B} \times 10^{-12}/T^B} \times 4.184 \times 10^2 \tag{15}$$

where the factor of 4.184×10^2 is necessary to give k_{fluid} in units of $W\ m^{-1}\ K^{-1}$.

The mass transfer, as mentioned previously, is the diffusion of oxygen through the surrounding film layer. This can be used in order to express the unknown, time dependent variable of $C_{O_2}\big|_{r_1}$ with the known constant value of $C_{O_2}^B$, the oxygen concentration of the bulk gas.

Mass transfer through the film layer is expressed as:

For $t \geq 0$:

$$R_C^* = k_g A \left(C_{O_2}^B - C_{O_2}\big|_{r_1} \right) \tag{16}$$

where R_C^* is the rate of oxygen diffusion, k_g the external diffusion coefficient, and $C_{O_2}^B$ the bulk gas oxygen concentration.

The rate of this external diffusion through the gas film layer is expressed using the external diffusion coefficient:

$$k_g = \frac{D_{O_2-CO} Sh}{2r_1} \tag{17}$$

where D_{O_2-CO} is the bulk diffusivity of oxygen through carbon monoxide, and Sh is the Sherwood number.

The Sherwood number, similarly to the Nusselt number, reduces to a value of 2 for a stagnant fluid [14]:

$$Sh = 2.0 \tag{18}$$

The bulk diffusivity, D_{O_2-CO}, is calculated using the formula given below [14]:

$$D_{O_2-CO} = \frac{1.8583 \times 10^{-3} T_{film}^{3/2} \sqrt{1/M_{O_2} + 1/M_{CO}}}{p \sigma_{O_2-CO}^2 \Omega} \tag{19}$$

where T_{film} is the temperature of the gaseous film surrounding the pellet assumed to be the average of bulk gas and surface temperatures, T^B and $T|_{r_1}$, M_{O_2} and M_{CO} are the molecular masses of oxygen and carbon dioxide, p is the pressure held at atmospheric pressure, σ_{O_2-CO} is a constant in the Lennard-Jones potential energy function with a value of 3.751Å and Ω is the collision integral. Assuming that the diffusing molecules are rigid spheres gives a value of $\Omega = 1$.

The concentration of oxygen at the uranium carbide surface $C_{O_2}\big|_{r_1}$ is then obtained in terms of the bulk gas oxygen concentration $C_{O_2}^B$ by equating Eqs. (5) and (16) for R_C and R_C^* respectively to give:

$$C_{O_2}\big|_{r_1} = \frac{k_g C_{O_2}^B}{k_g + k_1 exp\left(-E_A/RT|_{r_1}\right)} \tag{20}$$

This now allows the oxygen consumption rate at the reaction surface given in Eq. (5) to be expressed in terms of the bulk gas oxygen concentration:

$$R_C = \frac{k_1 exp\left(-E_A/RT|_{r_1}\right) A k_g C_{O_2}^B}{k_g + k_1 exp\left(-E_A/RT|_{r_1}\right)} \tag{21}$$

The boundary condition Eq. (11) now becomes

$$k_{UC} \frac{\partial T}{\partial r}\bigg|_{r_1} = h\left(T|_{r_1} - T^B\right) + \varepsilon\sigma\left(\left(T|_{r_1}\right)^4 - (T^B)^4\right) + \Delta H_R \frac{k_1 exp\left(-E_A/RT|_{r_1}\right) k_g C_{O_2}^B}{k_g + k_1 exp\left(-E_A/RT|_{r_1}\right)} \tag{22}$$

Expressing the external boundary condition in this manner allows its nonlinearity to be appreciated. This complicates the numerical solution which is discussed in the third section.

The Fourier Eq. (7) with the initial conditions Eqs. (8) and (9), and the boundary conditions Eqs. (10) and (22), therefore, complete the description of the heat transfer into and out of as well as throughout the pellet. Mass transfer across the film layer is described in Eq. (16),

and is then used to express the reaction rate, Eq. (5), in terms of the bulk oxygen concentration.

2.2 Calculating the Changing Pellet Size and Gas Composition

Eq.(21) provides the rate at which oxygen is consumed at the reaction interface. Using the stoichiometry of Eq. (1), this can be converted to the rate at which the uranium carbide depletes in $mol\ s^{-1}$:

For $t \geq 0$

$$\frac{dn_{UC}}{dt} = -\frac{R_C}{2} \tag{23}$$

where n_{UC} is the number of moles of uranium carbide.

The change in the number of moles of the uranium carbide can then be converted into a radial change by use of the molar density of uranium carbide, $\dot{\rho_{UC}}$.

Therefore, to complete the model, the radius of the spherical pellet diminishes with time according to the following expression:

$$\frac{dr_1}{dt} = -\frac{k_1 exp\left(-E_A/RT|_{r_1}\right) k_g C_{O_2}^B}{2\dot{\rho_{UC}}\left\{k_g + k_1 exp\left(-E_A/RT|_{r_1}\right)\right\}} \tag{24}$$

The non-linearity of Eq. (22) is now further exacerbated, because both the film heat and mass transfer coefficients, h and k_g, increase with time due their dependency on the reciprocal of the pellet radius.

The effect that the secondary oxidation described in Eq. (2) has on the composition of the bulk gas was also considered. The assumption that the bulk gas was infinite and stagnant was replaced with a finite and fixed volume, V, (for the majority of simulations, the volume was taken to be 1 m^3) that is not replenished.

The rate of reaction for the oxidation of carbon monoxide in air described in Eq. (2) is given by Howard et al [19]:

$$-\frac{dC_{CO}^B}{dt} = 1.3 \times 10^{14} [C_{CO}^B] \left[C_{O_2}^B\right]^{0.5} [H_2O]^{0.5} exp\left(\frac{-30}{RT^B}\right) \tag{25}$$

This produced a reaction rate in $mol\ ml^{-1}\ s^{-1}$ which was then converted to $mol\ \ s^{-1}$ by multiplying by the total volume of gas. The rate of CO_2 production was calculated using the stoichiometry of Eq. (2): for every mole of CO oxidised according to Eq. (25), a mole of CO_2 is produced. Oxygen depletion was included in the same fashion but combined with the effects of Eq. (1).

Figures 4a to 4c are plots of the changing number of moles of carbon monoxide and carbon dioxide in the bulk gas, as well as the number of moles of the solid carbide, at different bulk gas temperatures. In each case, the carbide is initially at room temperature, assumed here to be 20℃, and the bulk oxygen concentration is 3.15 $mol\ m^{-3}$ (corresponding roughly to the concentration of oxygen in air at a pressure of 1 atm). For the results depicted in Figures 4a, 4b and 4c, the assumption of an oxidant of infinite volume was removed.

At a bulk gas temperature of 20℃, no CO_2 is produced as it is too cool for the reaction rate in Eq. (25) to reach a significantly large value to oxidise the CO. At 300℃, the CO is completely oxidised after a small increase in concentration, and at 700℃ it is immediately oxidised to CO_2.

The effect that raising the bulk gas temperature has on increasing the rate at which the UC is consumed can also be observed in these figures.

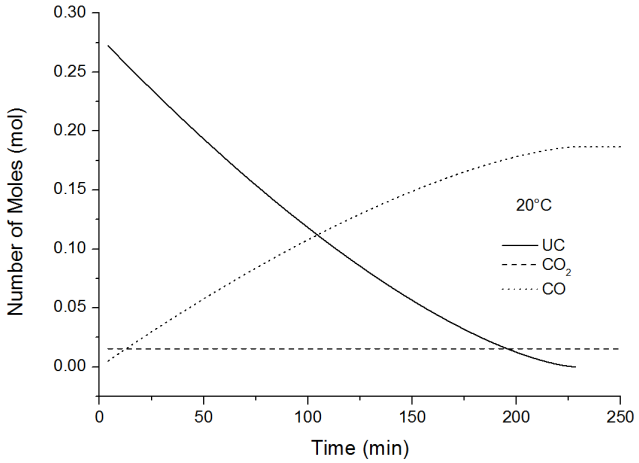

Fig. 4a. A plot of the change in the number of moles of UC, CO_2 and CO at a bulk gas temperature of 20℃

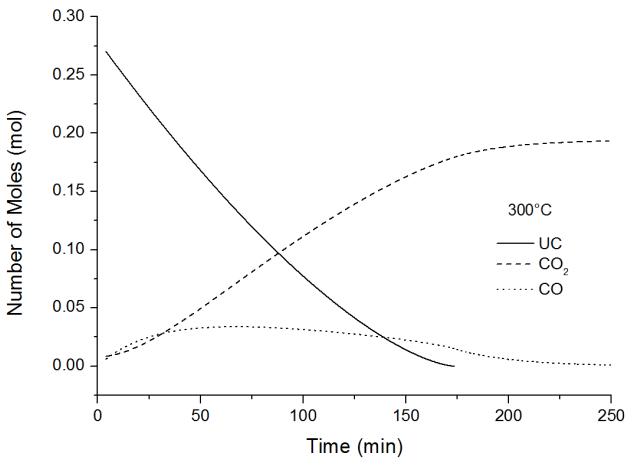

Fig. 4b. A plot of the change in the number of moles of UC, CO_2 and CO at a bulk gas temperature of 300℃

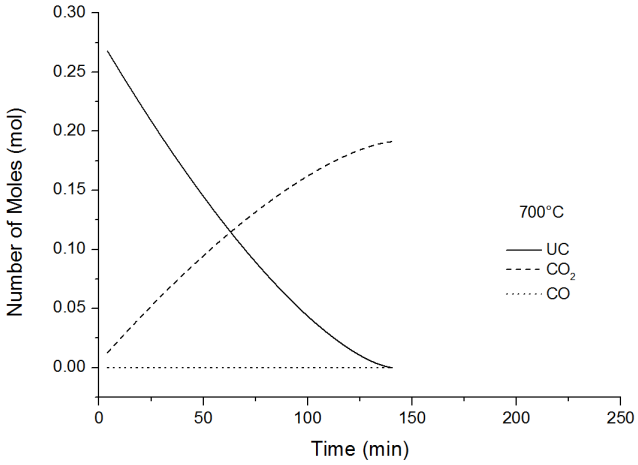

Fig. 4c. A plot of the change in the number of moles of UC, CO_2 and CO at a bulk gas temperature of 700℃

3 Numerical Solution

The results produced by the model, for example the plots illustrated in Figures 4a to 4c, were obtained from a numerical solution of the set of nonlinear partial and ordinary differential equations detailed in the previous section. These differential equations were solved by the application of finite-difference approximations, details of which are included in the following section.

3.1 Finite-Difference Method

The above equations were approximated using a finite-difference method known as the fully implicit backward (FIB) method [20].

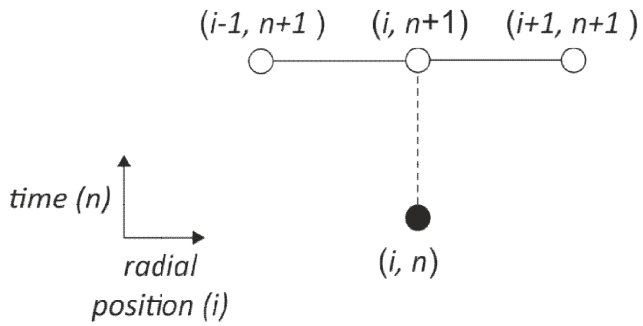

Fig. 5. The fully implicit backward finite-difference method. A known value, at a position i and a time step n, coloured black, is used to find values for the next time step $n+1$, coloured white, at the three radial positions, $i-1$, i, and $i+1$.

The FIB method calculates a solution at three different radial points for the next time step, $n+1$, using just a single value from the current time step, n, as illustrated in Figure 5.

The FIB finite-difference approximation of Eq. (7), the Fourier equation for heat transfer in a one dimensional sphere given by Eq. (26), is as follows:

For $n \geq 0$ and $2 \leq i \leq k-1$:

$$\frac{T_i^{n+1} - T_i^n}{\Delta t} = \alpha \left(\frac{v_i T_{i-1}^{n+1} - 2T_i^{n+1} + w_i T_{i+1}^{n+1}}{\Delta r^2} \right) \tag{26}$$

where Δr is the radial increment size across the carbide, Δt, is the time step size, $v_i = 1 - 1/i$ and $w_i = 1 + 1/i$ and i is an integer representing the radial position where $i = 1$ at the pellet centre and $i = k$, the number of radial increments, at the solid surface.

Eq. (26) is then applied across the solid. The number of radial increments, k, is held constant throughout the reaction, meaning that the radial increment size varies with time.

At the boundaries, where $i = 1$ or $i = k$, application of Eq. (26) creates imaginary points beyond the region on interest, $0 \leq r \leq r_1$. Finite-difference approximations of the boundary conditions must therefore be taken and applied to Eq. (26) at the relevant radial positions. When the appropriate boundary conditions and their finite-difference approximations have been taken into account, the resulting equations can be arranged into a tri-diagonal matrix. For this purpose, Eq. (26) is expressed in the form shown in Eq. (27) where the unknown terms are positioned on the left side of the equation:

For $n \geq 0$ and $2 \leq i \leq k-1$:

$$-M v_i T_{i-1}^{n+1} + (1 + 2M) T_i^{n+1} - M w_i T_{i+1}^{n+1} = T_i^n \tag{27}$$

where $M = \alpha \Delta t / \Delta r^2$.

3.1.1 Boundary Conditions – Adiabatic Central Condition

The boundary condition at the centre of the solid is considered first.

Eq. (7) cannot be used at $r = 0$, where $i = 1$, because the second term on the right hand side of the equation is indeterminate as ${}^{dT}/_{dr} = 0$ and $r = 0$. Applying L'Hôpital's rule to this term and setting $r = 0$ allows Eq. (7) to be expressed as:

For $t \geq 0$ and $r = 0$:

$$\frac{\partial T}{\partial t} = 3\alpha\left(\frac{\partial^2 T}{\partial r^2}\right) \tag{28}$$

Eq. (28), is then expressed as Eq. (29) after the FIB method is applied:

For $n \geq 0$ and $i = 1$:

$$\frac{T_1^{n+1} - T_1^n}{\Delta t} = 3\alpha\left(\frac{v_1 T_0^{n+1} - 2T_1^{n+1} + w_1 T_2^{n+1}}{\Delta r^2}\right) \tag{29}$$

The problem term in Eq. (29) is T_0^{n+1}, occurring at the imaginary point $i = 0$. In order to remove it a central difference approximation of the boundary condition from Eq. (10) is used. Central difference approximations are used due to the FIB approximation of the Fourier equation being second order. The resulting approximation can be found below in Eq. (30):

For $n \geq 0$ and $i = 1$:

$$\frac{T_2^n - T_0^n}{2\Delta r} = 0 \tag{30}$$

Substituting Eq. (30) into Eq. (27) to remove T_0^{n+1} gives an equation that can be inserted into the first row of the tri-diagonal matrix:

For $n \geq 0$ and $i = 1$:

$$(1 + 2M)T_1^{n+1} - 2MT_2^{n+1} = T_1^n \tag{31}$$

3.1.2. Boundary Conditions – Solid Surface

The other boundary condition requiring consideration is at the solid surface, where $i = k$. A central difference approximation is taken of Eq. (11):

For $n \geq 0$ and $i = k$:

$$\frac{T_{k+1}^n - T_{k-1}^n}{2\Delta r} = -\frac{h^n}{k_{UC}}(T_k^n - T^B) - \frac{\varepsilon\sigma}{k_{UC}}((T_k^n)^4 - (T^B)^4) - \frac{\Delta H_R}{k_{UC}}\frac{k_1 exp(-E_A/RT_k^n)k_g^n C_{O_2}^B}{k_g^n + k_1 exp(-E_A/RT_k^n)} \quad (32)$$

Rearranging this equation for T_{k+1}^n and subsituting that value into Eq. (27) with $i = k$ results in the following equation:

$$-2MT_{k-1}^{n+1} + \left(1 + 2M + 2Mu + \frac{2Mu}{h^{n+1}}\varepsilon\sigma(T_k^{n+1})^3\right)T_k^{n+1} + \frac{2Mu}{h^{n+1}}\varepsilon\sigma(T^B)^4 + \frac{2Mu\Delta H}{h^{n+1}}\frac{k_1 exp(-E_A/RT_k^{n+1})k_g^{n+1}C_{O_2}^B}{k_g^{n+1} + k_1 exp(-E_A/RT_k^{n+1})} = T_k^n + 2MuT^B \quad (33)$$

where $u = \Delta r w_k h/k_{UC}$.

Eq. (33), however, is nonlinear as solving for T^{n+1} requires prior knowledge of T_k^{n+1} in order to calculate the heat of reaction and radiation terms present. It must therefore be linearised by multiplying both the numerator and denominator of the heat of reaction term by T_k^{n+1}, allowing it to take the tri-diagonal form shared by Eqs. (27) and (31). The calculation is then iterated a number of times until a set tolerance limit is reached. For the first iteration, R_C is calculated assuming $T_k^{n+1} = T_k^n$. The solution is then recalculated at the same time step using the newly calculated value for T_k^{n+1}. Letting z represent the number of iterations starting at $z = 1$, Eq. (33) is re-written as:

$$-2MT_{k-1}^{n+1,z+1} + \left\{1 + 2M + 2Mu + \frac{2Mu}{h^{n+1}}\varepsilon\sigma\left(T_k^{n+1,z}\right)^3 + \frac{2Mu}{h^{n+1}T_k^{n+1,z}}\varepsilon\sigma(T^B)^4 + \frac{2Mu\Delta H}{h^{n+1}T_k^{n+1,z}}\frac{k_1 exp\left(-E_A/RT_k^{n+1,z}\right)k_g^{n+1}C_{O_2}^B}{k_g^{n+1} + k_1 exp\left(-E_A/RT_k^{n+1,z}\right)}\right\}T_k^{n+1,z+1} = T_k^n + 2MuT^B \quad (34)$$

This iterative process is then carried out until the following criterion is satisfied:

$$\frac{T_k^{n+1,z+1} - T_k^{n+1,z}}{T_k^{n+1,z+1}} < Tolerance\ for\ all\ temperatures \quad (35)$$

The tolerance can be set to any value, generally around 0.1%, with the solution becoming more stable as it is decreased.

A further iterative step is also required due to the heat and mass transfer coefficients, h and k_g respectively, being dependent on the radius adding further nonlinearity to the solution.

To solve the tri-diagonal matrix, values of h^{n+1} and k_g^{n+1}, present in Eq. (34), are required but are dependent on the radial increment size which is only known at the current time step, n. Similarly to the iteration of the temperature values, h^{n+1} and k_g^{n+1} are solved assuming $r^{n+1} = r^n$, and the entire solution, including the final radial change, is iteratively recalculated until a criterion similar to that in Eq. (35), but applied to the radius, is satisfied.

The resulting tri-diagonal matrices were then solved using the Thomas algorithm [21] in original code written in FORTRAN 95, providing the temperature distributions at the time step $n + 1$. This information could then be used to calculate the new carbide radius, r_1, at each time step using a backward difference approximation of Eq. (24):

$$r_1^{n+1} = r_1^n - \frac{\Delta t k_1 exp\left(-E_A/RT^{n+1}|_{r_1}\right) k_g^{n+1} C_{O_2}^B}{2\rho_{UC}\left\{k_g^{n+1} + k_1 exp\left(-E_A/RT^{n+1}|_{r_1}\right)\right\}} \tag{36}$$

The time loop was continued until the percentage of carbide oxidised became greater than 99%.

3.2 Ensuring Numerical Stability

When using finite-difference methods, it is vital to ensure that the solution remains stable so that the output can be trusted. The general stability criteria used in this work is the Courant-Friedrichs-Lewy rule [20], adapted for the various constants and increment sizes that affect stability in this particular case.

$$\Delta t = \frac{1}{2\alpha}\Delta r^2 \tag{37}$$

The time step size is recalculated at every time step. The new values for the radial increment sizes and thermal and mass diffusion constants are worked out using the previous solution, including the iteration of the temperature and radial increment size, and applied to Eq. (37) to calculate the time step size. The solution is then converged using this time step and the process is repeated. Through this careful control of the time step size, it is ensured that the solution remains stable throughout.

3.3 Checking for Convergence

In order to check for mathematical convergence, the model was run using the same input parameters but using a different number of radial increments and hence different values for the initial increment size. The results of this are listed in Table 1. The minor changes observed in the solution upon varying the initial increment size revealed that the model is convergent, especially when more than 50 increments are used.

Number of Radial Increments	Oxidation Completion Time (min)	Computational Time (s)
5	261.8	0.2028
10	262.3	0.5772
20	262.5	2.995
50	262.5	34.66
100	262.5	250.2
200	262.6	1984

Table 1. The effect of varying the number of increments on the oxidation completion time as a test for convergence.

Richardson's deferred approach to the limit [20] can be used in this case to extrapolate the results from three different increment sizes to predict the solution for an infinitely small increment size. Taking the first three results from Table 1 and applying them to Eqs. (38) and (39) allows the prediction of such a solution:

$$u = \frac{h_2^p u_1 - h_1^p u_2}{h_2^p - h_1^p} \tag{38}$$

where u_1 and u_2 are the solutions (completion times) at initial radial increment sizes of h_1 and h_2, and p can be calculated from:

$$2^p = \frac{u_2 - u_1}{u_3 - u_2} \tag{39}$$

where u_3 is the solution at h_3, and $h_3 = \frac{1}{2}h_2 = \frac{1}{4}h_1$.

A value of $p = 1.322$ is obtained, leading to the calculation of $u = 262.6\ min$. This allows the conclusion that the model successfully converges on the solution as the number of increment sizes is increased.

4 Results

The complete oxidation model is capable of predicting the reaction completion time and the transient temperature distribution throughout the solid over the course of the reaction. An example of these capabilities can be seen in Figure 6a which displays the temperature distribution throughout the solid and the reduction in the solid radius over time, as well as the overall reaction completion time. Figure 6b examines the radial temperature gradient more closely at two instances of time during the reaction. For both Figures, a pellet of radius 0.935 cm initially assumed to be at 25°C is exposed to a bulk gas of a volume of 1 m^3 at an initial temperature of 500°C. The bulk gas is taken to be air at 1 atm with an oxygen concentration of 3.15 $mol\ m^{-3}$. These conditions were chosen to represent how the oxidation could be realistically carried out.

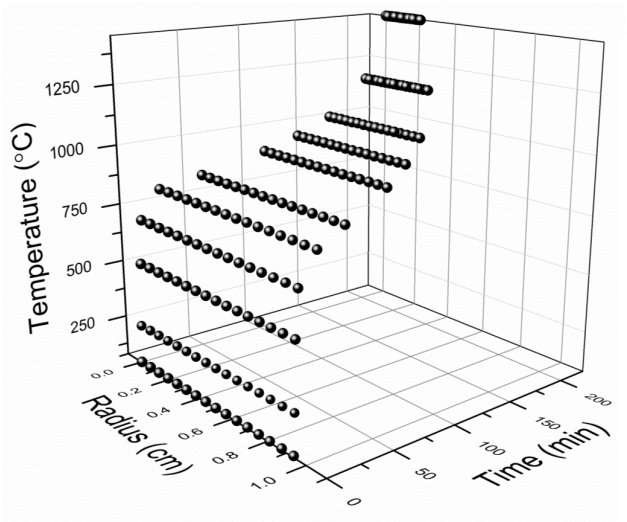

Fig. 6a. Radial temperature distribution over time illustrating both the shrinking radius and the thermal response of the pellet.

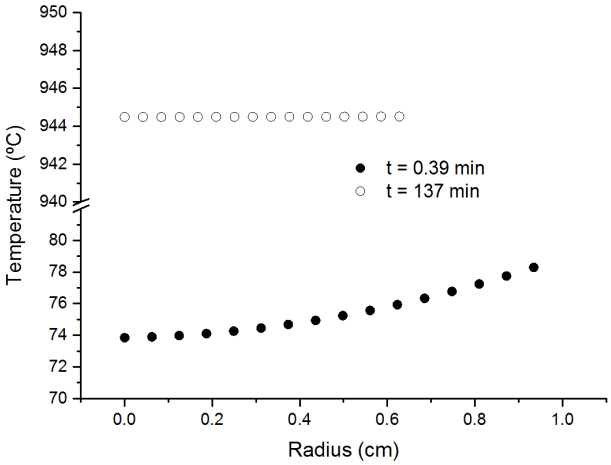

Fig. 6b. Two instantaneous temperature profiles plotting the temperature gradient across the carbide radius. .

In Figure 6a, an initial steep increase in the temperature along the radius is observed as the pellet experiences a large convective heat flux at the surface due to exposure to the hotter bulk gas. It overshoots the bulk gas temperature, however, due to the generation of heat from the oxidation reaction. There is then a rough plateau for the majority of the reaction as the heat generation is similar to the heat lost to the bulk gas. This is in part due to the effect of radiative heat loss becoming more significant at higher temperatures. Then, toward the end of the reaction as the pellet's radius becomes small, there is a temperature spike and a degree of thermal runaway.

Figure 6b, a plot of two radial temperature profiles taken at different times during the reaction, illustrates the radial temperature gradient in the carbide in more detail. Initially, when the pellet is exposed to the hotter bulk gas, a temperature gradient exists with the surface of the carbide being hotter. As the reaction proceeds however, the temperature

gradient becomes minimal due to the high conductivity of uranium carbide, as illustrated in the plot at $t = 137\ min$.

The ignition effect displayed in Figure 6a can be explained through examination of the competing heat fluxes acting on the pellet: the heat generated by the reaction and the heat exchanged with the bulk gas. Figure 7 displays the heat exchanged with the bulk gas subtracted from the heat generated to create a value that is then compared against the surface temperature of the pellet over time.

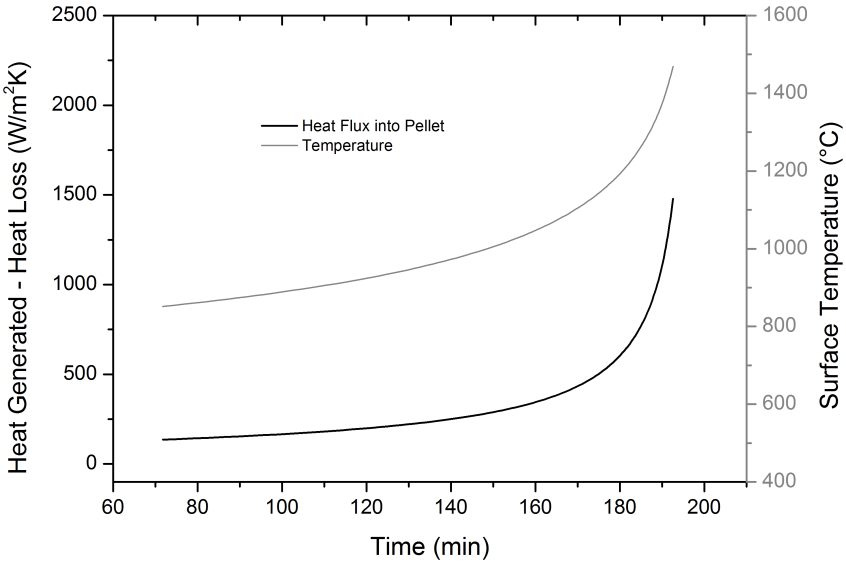

Fig. 7. A plot of the difference between the heat generated and the heat lost to the bulk gas in black, and the surface temperature of the pellet in grey, against time. The plot is taken from the latter stages of the reaction to concentrate on the region of interest.

In Figure 7 the net heat flux into the pellet becomes greater towards the end of the reaction, hence the sharp rise in surface temperature. This is due to heat generation from the reaction having a greater temperature dependence on the surface temperature than the heat loss via radiation and convection and therefore increases in magnitude faster with the steadily increasing surface area. The effect of the heat into the system becoming larger than the heat out can be considered an ignition according to Babrauskas [22].

Sensitivity studies were carried out with the model to investigate the effects of varying the input parameters, such as bulk gas temperature and oxygen concentration, on the temperatures reached and reaction completion time.

Figure 8 is a plot showing how the surface temperature of the carbide pellet and the fraction of carbide oxidised increase over time. Each relationship is presented at three different bulk gas temperatures so that the effects of varying it can be observed. The oxygen concentration was again assumed to be 3.15 $mol\ m^{-3}$, the radius to be 0.935 cm and the initial temperature of the pellet was 25°C. Table 2 provides more quantitative detail of the results.

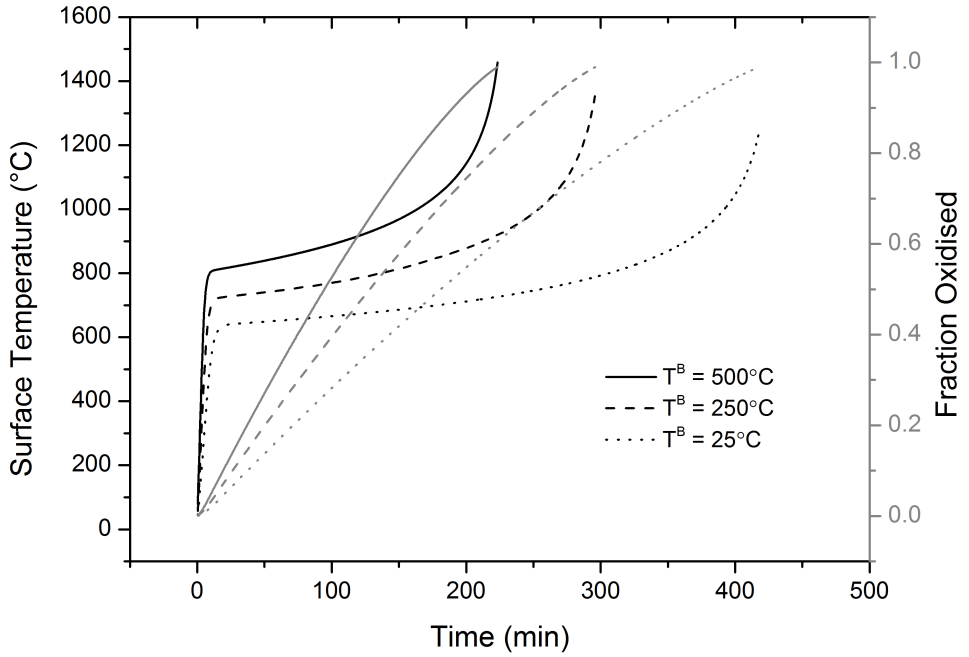

Fig. 8. The surface temperature of the carbide, represented by the line and y-axis in black, and the fraction oxidised, represented by the line and y-axis in grey, versus time. Three oxidations were simulated at different initial bulk gas temperatures of 25, 250 and 500°C.

Initial Bulk Gas Temperature (°C)	Peak Surface Temperature (°C)	Reaction Completion Time (min)	Final Bulk Gas Temperature (°C)
25.0	1253	418	57.0
250.0	1365	296	381.0
500.0	1458	223	644.8

Table 2. A table showing how the bulk gas temperature affects the peak surface temperature reached by the carbide, the reaction completion time and the final bulk gas temperature.

Figure 8 and Table 2 indicate that increasing the initial temperature of the oxidising gas greatly decreases the reaction completion time, whilst also having a significant effect on the peak temperature reached. There is also a more significant increase in the final bulk gas temperature, most likely due to the hotter pellet and a faster rate of carbon monoxide oxidation in the gas.

Figure 9 is a similar graph illustrating the effects of different bulk oxygen concentrations, using an initial bulk gas temperature of 250°C and the same initial pellet conditions. Table 3 provides the numerical results.

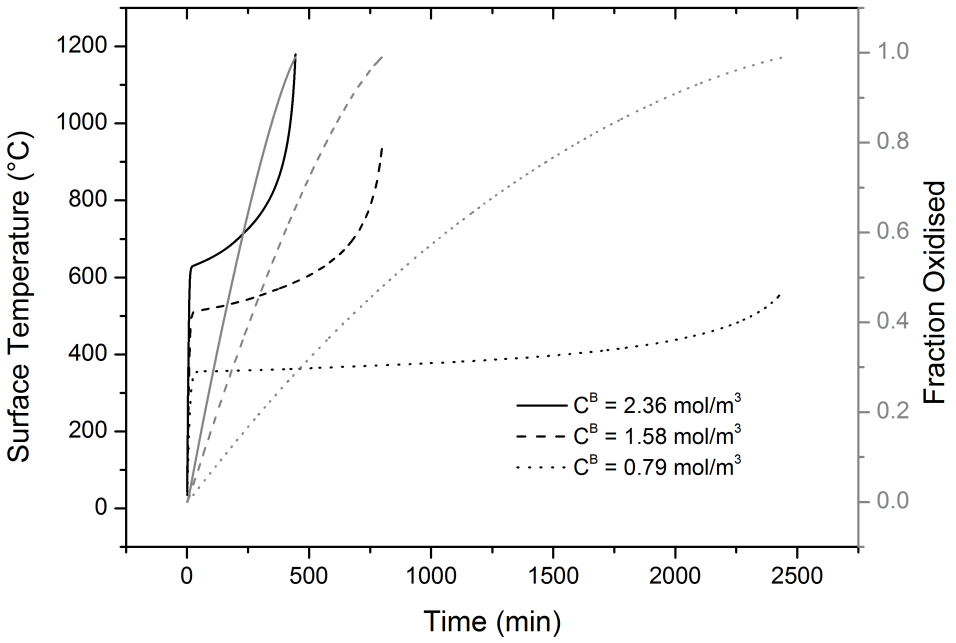

Fig. 9. The surface temperature of the carbide (black) and the fraction oxidised (grey) versus time, carried out at bulk gas oxygen concentrations of 0.788, 1.58 and 2.36$mol\ m^{-3}$. An initial bulk gas temperature of 250°C was used in each case.

Bulk Gas Oxygen Concentration ($mol\ m^{-3}$)	Peak Surface Temperature (°C)	Reaction Completion Time (min)	Final Bulk Gas Temperature (°C)
0.788	563.5	2442	657.6
1.58	938.4	798.7	673.5
2.36	1179	444.2	663.2

Table 3. The effects of the bulk gas oxygen concentration on the peak surface temperature, reaction completion time and the final bulk gas temperature at an initial bulk gas temperature of 250°C.

Figure 9 and Table 3 illustrate that increasing the oxygen concentration in the bulk gas has a similar effect to increasing the temperature. When reduced to 0.788 $mol\ m^{-3}$, the rate of oxidation is slowed significantly causing a much more modest temperature increase. The effects on the final bulk gas temperature are also slightly more unpredictable, as both the amount of time available for the secondary oxidation and the temperature at which it is occurring are factors.

The effect of decreasing the volume of oxidising fluid was also investigated. Due to the time dependent decrease of the oxygen concentration in the total bulk fluid according to Eq. (21), a minimum volume required for complete oxidation of the carbide can be found. Figure 10

displays the effect of varying the volume of the bulk fluid on the fraction oxidised. At a bulk gas volume of 1 m^3, the relative oxygen consumption is minimal. When the volume of gas is decreased to 0.2 m^3, the change in rate of reaction is small, but there is a large decrease in the final oxygen concentration; from 2.78 $mol\ m^{-3}$ at $V = 1\ m^3$ to 1.31 $mol\ m^{-3}$ at $V = 0.2\ m^3$. If the volume is decreased by a factor of 10, to 0.1 m^3, there is not enough oxygen present in the bulk gas to complete the oxidation.

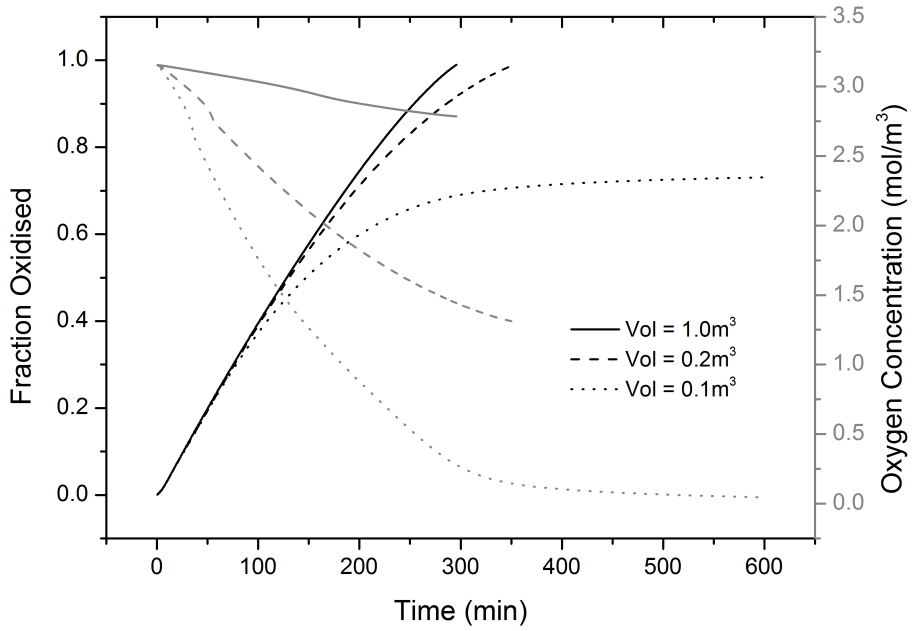

Fig. 10. The fraction oxidised in black and the oxygen concentration in the bulk gas in grey versus time.

In summary, the model predicts for a typical orthocylindrical pellet size of $9.35\ mm$ that the oxidation generally takes between 200-2000 minutes depending on the input parameters. Temperatures in the pellet reach a maximum as the reaction completes and reached 1458°C when the bulk gas was set to 500°C, highlighting the high exothermicity of the reaction. Lower oxygen concentrations and bulk gas temperatures can reduce the temperature rise significantly. For example, a relatively small temperature peak of 563°C at an initial gas temperature of 250°C and oxygen concentration of 0.788 $mol\ m^{-3}$ could suggest that these values represent safe operating conditions for the oxidation.

5. Conclusions

A transient mathematical model with a moving-boundary for the oxidation of a UC pellet coupled with a secondary oxidation of CO included in the surrounding gas phase is developed. The model for the UC is represented by the Fourier equation at any instant of time with a non-linear boundary condition at the outer surface that moves with time. This boundary condition accommodates the non-linear reaction rate term for the diffusion of species to and from the outer surface as well as heat transfer by convection and thermal radiation.

The partial and ordinary differential equations of the model are solved numerically by the application of implicit and explicit finite difference approximations. The resulting set of non-linear algebraic equations is highly non-linear, as shown in Eq. (34), and linearization is used to obtain a solution at each time increment. Convergence at each time step is enforced before proceeding to the next time increment.

The numerical stability of the model is controlled by a dynamic time step size calculated from the Courant-Friedrichs-Lewy condition, which accommodates the change in the size of the radial increment. The numerical solution is checked for convergence by progressively increasing the number of radial increments and using Richardson's deferred appproach to the limit methodology.

Reaction rate and completion time, temperature profiles in the pellet and gas composition changes can be predicted. Sensitivity studies have been carried out to establish the effect the input parameters can have on the predicted results.

The model differs from the only other model of this reaction that is available in the open literature in that the oxide product is not adherent, as is suggested by Mazuadier [11] and by Mukerjee [10] when higher O_2 partial pressures are applied (≥20kPa). The model is therefore significant to the field by virtue of being valid at different conditions to Scott's model [15], and also by comprehensively generating a stable and convergent numerical solution of the system.

Further work will include examining the oxidation using more advanced approaches with the ability to model the system in three dimensions, to model batch oxidations and also to simulate fluid flow around the system.

6 Acknowledgements

The research leading to the results contained in this paper received funding from the European Union 7th Framework Programme FP7-Fission-2011-2.3.1 under grant agreement number 295825 (Project ASGARD). The paper reflects only the authors' views and the European Union is not liable for any use that may be made of the information contained therein.

7 References

1. Legand, S., C. Bouyer, V. Dauvois, F. Casanova, D. Lebeau, and C. Lamouroux, *Uranium carbide dissolution in nitric acid: speciation of organic compounds.* Journal of Radioanalytical and Nuclear Chemistry, 2014. **302**(1): p. 27-39.
2. Raveu, G., G. Martin, O. Fiquet, P. Garcia, G. Carlot, H. Palancher, A. Bonnin, H. Khodja, C. Raepsaet, T. Sauvage, and M.-F. Barthe, *Experimental study of UC polycrystals in the prospect of improving the as-fabricated sample purity.* Nuclear Instruments and Methods in Physics Research Section B: Beam Interactions with Materials and Atoms, 2014. **341**(0): p. 72-76.
3. De Coninck, R., W. Van Lierde, and A. Gijs, *Uranium carbide: Thermal diffusivity, thermal conductivity and spectral emissivity at high temperatures.* Journal of Nuclear Materials, 1975. **57**(1): p. 69-76.
4. Carbajo, J.J., G.L. Yoder, S.G. Popov, and V.K. Ivanov, *A review of the thermophysical properties of MOX and UO2 fuels.* Journal of Nuclear Materials, 2001. **299**(3): p. 181-198.
5. Ferris, L.M., M.J. Bradley, and U.S.A.E. Commission, *Off-gases from the reactions of uranium carbides with nitric acid at 90°C*. ORNL ;3719. 1964, Oak Ridge, Tenn.: Oak Ridge National Laboratory. iii, 19 p.
6. Ferris, L.M. and M.J. Bradley, *Reactions of Uranium Carbides with Nitric Acid.* The Journal of American Chemistry, 1965. **87**.
7. Macleod, H.M., *Review of Experience in Converting Oxidation (U, Pu)C to (U, Pu)O by CO2*, 1997, BNFL Report. p. 142.
8. Dell, R.M. and V.J. Wheeler, *The ignition of uranium mononitride and uranium monocarbide in oxygen.* Journal of Nuclear Materials, 1967. **21**(3): p. 328-336.
9. Le Guyadec, F., C. Rado, S. Joffre, S. Coullomb, C. Chatillon, and E. Blanquet, *Thermodynamic and experimental study of UC powders ignition.* Journal of Nuclear Materials, 2009. **393**(2): p. 333-342.
10. Mukerjee, S.K., G.A.R. Rao, J.V. Dehadraya, V.N. Vaidya, V. Venugopal, and D.D. Sood, *The oxidation of uranium monocarbide microspheres.* Journal of Nuclear Materials, 1994. **210**(1–2): p. 97-106.
11. Mazaudier, F., C. Tamani, A. Galerie, and Y. Marc, *On the oxidation of (U,Pu)C fuel: Experimental and kinetic aspects, practical issues.* Journal of Nuclear Materials, 2010. **406**(3): p. 277-284.
12. Berthinier, C., S. Coullomb, C. Rado, E. Blanquet, R. Boichot, and C. Chatillon, *Experimental study of uranium carbide pyrophoricity.* Powder Technology, 2011. **208**(2): p. 312-317.
13. Berthinier, C., S. Coullomb, C. Rado, F. LeGuyadec, C. Chatillon, E. Blanquet, and R. Boichot. *Experimental thermal analysis of uranium carbide powder ignition*. in *Proceedings of Global*. 2009.
14. Smith, J.M., *Chemical Engineering Kinetics*. 1970: McGraw-Hill.

15. Scott, C.D., *Analysis of Combustion of Graphite-Uranium Fuels in a Fixed Bed or Moving Bed.* Industrial & Engineering Chemistry Process Design and Development, 1966. **5**(3): p. 223-233.

16. Naito, K., N. Kamegashira, T. Kondo, and S. Takeda, *Isothermal Oxidation, of Uranium Monocarbide Powder under Controlled Oxygen Partial Pressures.* Journal of Nuclear Science and Technology, 1976. **13**(5): p. 260-267.

17. P. N. Rowe, K.T.K., J. B. Lewis, *Heat and mass transfer from a single sphere in an extensive flowing fluid.* Chemical Engineering Research and Design, 1965. **43a**: p. 14-31.

18. Vines, R.G., *Measurement of the Thermal Conductivities of Gases at High Temperatures.* Journal of Heat Transfer, 1960. **82**(1): p. 48-52.

19. Howard, J.B., G.C. Williams, and D.H. Fine, *Kinetics of carbon monoxide oxidation in postflame gases.* Symposium (International) on Combustion, 1973. **14**(1): p. 975-986.

20. Smith, G.D., *Numerical Solution of Partial Differential Equations*. 1965: Oxford University Press.

21. Chang, H.-Y., *Selected Numerical Methods and Computer Programs for Chemical Engineers*. 1981: Sterling Swift Pub Co. 84-89.

22. Babrauskas, V., *Ignition Handbook*. 2003: Fire Science Publishers.